Decorative near-infrared transmission filters featuring high-efficiency and angular-insensitivity employing 1D photonic crystals

Chengang Ji[1], Chenying Yang[1,2], Weidong Shen[2,*], Kyu-Tae Lee[3], Yueguang Zhang[2], Xu Liu[2], and L. Jay. Guo[1,*]

[1]Department of Electrical Engineering and Computer Science, The University of Michigan, USA

[2]State Key Laboratory of Modern Optical Instrumentation, Department of Optical Engineering, Zhejiang University, China

[3]Department of Physics, Inha University, Republic of Korea

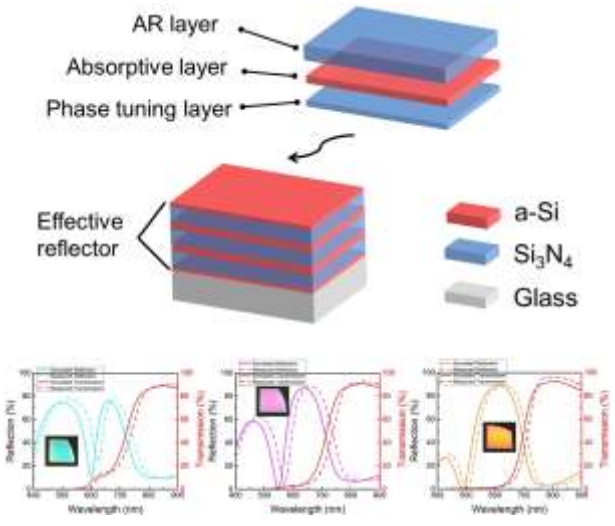

Decorative visibly-opaque but near-infrared-transmitting filters that possess high-efficiency and angular-insensitivity are demonstrated employing one-dimensional ternary photonic crystals. Different reflective colors can be generated without affecting the near-infrared transmission performance, thus opening up new possibilities for a wide variety of applications such as image sensors, optical detections, and NIR decorations.

Nano Research

ISSN 1998-0124 CN 11-5974/O4
https://doi.org/(automatically inserted by the publisher)

Decorative near-infrared transmission filters featuring high-efficiency and angular-insensitivity employing 1D photonic crystals

Chengang Ji[1,§], Chenying Yang[1,2,§], Weidong Shen[2] (✉), Kyu-Tae Lee[3], Yueguang Zhang[2], Xu Liu[2], and L. Jay. Guo[1] (✉)

[1] *Department of Electrical Engineering and Computer Science, The University of Michigan, Ann Arbor, Michigan 48109, USA*
[2] *State Key Laboratory of Modern Optical Instrumentation, Department of Optical Engineering, Zhejiang University, Hangzhou 310027, China*
[3] *Department of Physics, Inha University, Incheon 22212, Republic of Korea*
[§] *Chengang Ji and Chenying Yang contributed equally to this work*

Received: day month year / **Revised:** day month year / **Accepted:** day month year (automatically inserted by the publisher)

ABSTRACT

We present a new scheme for visibly-opaque but near-infrared-transmitting filters involving 7 layers based on one-dimensional ternary photonic crystals, with capabilities in reaching nearly 100% transmission efficiency in the near-infrared region. Different decorative reflection colors can be created by adding additional three layers while maintaining the near-infrared transmission performance. In addition, our proposed structural colors show great angular insensitivity up to ±60° for both transverse electric and transverse magnetic polarizations, which are highly desired in various fields. The facile strategy described here involves a simple deposition method for the fabrication, thereby having great potential in diverse applications such as image sensors, anti-counterfeit tag, and optical measurement systems.

KEYWORDS

NIR-transmitting filters, colored decorations, photonic crystals, multilayer structures

1 Introduction

Visibly-opaque but near-infrared (NIR)-transmitting filters have received considerable interest due to their irreplaceable roles in various applications including NIR spectroscopy, security imaging, optical detections, to name an important few [1-8]. In recent years, decorative NIR filters that exhibit aesthetic colors are also highly desired to both enhance the signal-to-noise ratio and hide the unappealing appearance of sensors (*e.g.*, proximity sensors, gesture sensors, and camera monitoring systems) integral to advanced technologies that are closely related to our daily life, such as vehicles, cell phones, etc. Organic dyes or pigments that can absorb ultraviolet (UV) and visible light but transmit NIR waves provide one option [9-11]. However, these organic materials suffer from short life-time problems due to their susceptibility to environmental factors such as moisture, high temperature and constant UV exposure. Structural NIR-transmitting filters that are patterned at the subwavelength scale to excite either guided-mode resonance (GMR) or surface plasmon polariton (SPP) have been demonstrated to address the aforementioned challenges [12-18]. The coupling of incident light into those resonances needs to be achieved with the subwavelength gratings, which require complicated fabrication procedures such as e-beam lithography and focused ion beam milling, rendering them difficult for large-area applications. Moreover, the resulting transmission spectra are highly sensitive to an angle of incidence due to the momentum matching condition, thereby dramatically limiting their potential for many applications. A more cost-effective and widely-adopted method to create NIR transmission while blocking the visible light is using one-dimensional (1D) photonic crystals (PCs), which are made of periodic layered structures consisting of alternating high and low index materials [5, 19-25]. By locating the passband in the NIR range while the stopband in the visible, adjustable NIR transmission performance can be achieved by selecting different constituent materials and layer thicknesses. However, as the structures based on single-periodic stacks have very limited stopband bandwidth, stacking of different period units are typically required to produce overlapping multiple stopbands to broaden the stopband, in order to block all the visible light transmission. As a result, these PC-based filters typically involve tens or even hundreds of layers, which faces the manufacturing cost and yield issues.

In this work, we report a new approach for colored NIR transmission filters that blocks the visible light, with the option to create desired color reflection. The design exploits 1D ternary PCs involving 7 layers. Simultaneously, taking the advantage of the absorptive property of the constituent semiconductor (*e.g.*, a-Si) in the visible range, various reflection colors, not limited to the one complementary to the transmissive spectrum, can be

Address correspondence to L. Jay Guo, guo@umich.edu; Weidong Shen, adongszju@hotmail.com

generated without affecting the transmission performance, which can be used for decoration applications and 'hide' objects behind the filters. The proposed structural color exhibits ultrahigh transmission efficiency with the maximum close to 100% and angle invariant property up to ±60° regardless of the polarization state of incident light from both illumination directions due to the low loss and high refractive indices of the materials used, surpassing the performance of many previous works. An additional advantage of the proposed structural colors lies in their simplicity where only thin film deposition is required for the fabrication, thus enabling large-scale manufacturing for practical applications. The approach described in this work could open up many potential applications such as imaging sensors, optical measurement systems, and decorations.

2 Results and discussion

2.1 Proposed Visibly-Opaque but NIR-Transmitting Filters

A schematic diagram of the proposed structure featuring angular- and polarization-independent NIR transmission is depicted in Fig. 1(a). It is targeted at high transmissive efficiency employing three stacks of $'H/2LH/2'$ unit as an effective AR coating based on Herpin's equivalent index [19, 26]. Here, H and L denote the high and low refractive index materials with a quarter-wavelength thickness, separately (*i.e.*, $H=\lambda_c/4n_H$ and $L=\lambda_c/4n_L$). Selecting a central wavelength of the stopband as λ_c = 550 nm and amorphous silicon (a-Si, $n_H=4.4+i0.27$) and silicon nitride (Si_3N_4, $n_L=1.9$) as H (~ 32 nm) and L (~ 72 nm) layers, respectively, the stopband bandwidth can be calculated from $\Delta(\lambda_c/\lambda)=(4/\pi)\sin^{-1}[(n_H-n_L)/(n_H+n_L)]$ with the left and right band edge located at λ_L = 430 nm and λ_R = 740 nm, respectively (Fig. 1(b)) [19]. It should be noted that both H and $\Delta\lambda$ are approximated using the real part of refractive index of a-Si in the calculation considering its small but nonzero extinction efficiency [19]. It is easy to understand from the above equation that such a broad stopband is a direct consequence of the high index contrast between the high (a-Si) and low (Si_3N_4) index materials used in the design. Due to the wide range stopband together with the semiconductor loss, visible incidence (wavelength < 650 nm) is effectively blocked with only 7 layers as shown by the spectra in Fig. 1(b). As a result, the fabricated samples showing mirror-like bright reflection (inset at the bottom-left corner). As a comparison, the simulated reflection and transmission spectra of the 7-layered PC structure based on lower refractive index material combinations (*i.e.*, employing titanium dioxide (TiO_2) and silicon dioxide (SiO_2) as the high and low index materials, respectively), is given in Fig. S1 in the Electronic Supplementary Material (ESM). It is obvious that its stopband bandwidth is much narrower and visible light can pass through the stacks even within the stopband range. The thickness of TiO_2/SiO_2 is designed so that the center wavelength of the stopband is located at the same position (λ_c = 550 nm). Due to the negligible absorption loss of both a-Si and Si_3N_4 materials beyond 700 nm, high transmission close to unity (99.88% @735 nm) can be achieved at normal incidence in NIR range as plotted in Fig. 1(b) showing excellent agreement between the calculated and measured results. Here, the simulations based on the transfer matrix method [27] with the refractive indices of materials (Fig. S2 in the ESM) calibrated using a spectroscopic ellipsometer (M-2000, J. A. Woollam) are performed, and the reflection and transmission spectra are measured by using the spectrophotometer (Cary 7000, Agilent). Both a-Si and Si_3N_4 are deposited with plasma-enhanced chemical vapor deposition (PECVD) at 260 °C alternatively without breaking the vacuum chamber. We note that the measured transmission is slightly lower than the calculations and this can be attributed to the reflection at the interface between the air and the bottom of the fused silica substrate, which has not been considered in the simulations. Due to the symmetric configuration of the proposed structure, the stacks exhibit the same performance at both top and bottom illuminations, which can further extend our design into more applications, such as color pigments.

2.2 Angular-Insensitive Optical Performance

For ternary PCs consisting of the '$H/2LH/2$' unit, the characteristic matrix of one period is

$$\vec{\vec{M}}=\begin{pmatrix} & M_{12} \\ M_{21} & M_{22} \end{pmatrix},$$

with

Nano Research
ISSN 1998-0124 CN 11-5974/O4
https://doi.org/(automatically inserted by the publisher)

$$M_{11}=\cos 2k_{H,x}\cos k_{L,x}-\frac{1}{2}\left(\frac{k_{L,x}}{k_{H,x}}+\frac{k_{H,x}}{k_{L,x}}\right)\sin 2k_{H,x}\sin k_{L,x}$$

$$M_{12}=\frac{k_0H/2}{ik_{H,x}}\left[\sin 2k_{H,x}\cos k_{L,x}+\frac{1}{2}\left(\frac{k_{L,x}}{k_{H,x}}+\frac{k_{H,x}}{k_{L,x}}\right)\cos 2k_{H,x}\sin k_{L,x}+\frac{1}{2}\left(\frac{k_{H,x}}{k_{L,x}}-\frac{k_{L,x}}{k_{H,x}}\right)\sin k_{L,x}\right]$$

$$M_{21}=-i\frac{k_{H,x}}{k_0H/2}\left[\sin 2k_{H,x}\cos k_{L,x}+\frac{1}{2}\left(\frac{k_{L,x}}{k_{H,x}}+\frac{k_{H,x}}{k_{L,x}}\right)\cos 2k_{H,x}\sin k_{L,x}-\frac{1}{2}\left(\frac{k_{H,x}}{k_{L,x}}-\frac{k_{L,x}}{k_{H,x}}\right)\sin k_{L,x}\right]$$

$$M_{22}=M_{11}$$

for TE polarization, and

$$M_{11}=\cos 2k_{H,x}\cos k_{L,x}-\frac{1}{2}\left(\frac{n_H^2k_{L,x}}{n_L^2k_{H,x}}+\frac{n_L^2k_{H,x}}{n_H^2k_{L,x}}\right)\sin 2k_{H,x}\sin k_{L,x}$$

$$M_{12}=\frac{n_H^2k_0H}{2ik_{H,x}}\left[\sin 2k_{H,x}\cos k_{L,x}+\frac{1}{2}\left(\frac{n_H^2k_{L,x}}{n_L^2k_{H,x}}+\frac{n_L^2k_{H,x}}{n_H^2k_{L,x}}\right)\cos 2k_{H,x}\sin k_{L,x}+\frac{1}{2}\left(\frac{n_L^2k_{H,x}}{n_H^2k_{L,x}}-\frac{n_H^2k_{L,x}}{n_L^2k_{H,x}}\right)\sin k_{L,x}\right]$$

$$M_{21}=\frac{-2ik_{H,x}}{n_H^2k_0H}\left[\sin 2k_{H,x}\cos k_{L,x}+\frac{1}{2}\left(\frac{n_H^2k_{L,x}}{n_L^2k_{H,x}}+\frac{n_L^2k_{H,x}}{n_H^2k_{L,x}}\right)\cos 2k_{H,x}\sin k_{L,x}-\frac{1}{2}\left(\frac{n_L^2k_{H,x}}{n_H^2k_{L,x}}-\frac{n_H^2k_{L,x}}{n_L^2k_{H,x}}\right)\sin k_{L,x}\right]$$

$$M_{22}=M_{11}$$

for TM polarization [19, 28-30]. $k_{H,x}=k_0n_HH\cos\theta_H/2$ and $k_{L,x}=k_0n_LL\cos\theta_L/2$ are the wave vectors along the x direction for the waves propagating in the high and low refractive index layers, respectively, $k_0=\omega(\varepsilon_0\mu_0)^{1/2}$ is the free-space wave vector with ω as the frequency of incident light, and $\theta_{H(L)}$ is the corresponding propagation angle in each layer determined by the Snell's law. Based on the characteristic matrix, the projected band structure for both polarizations can be calculated from the Bloch wave number $K(\omega,\beta)=\cos^{-1}[M_{11}+M_{22}/2]/\Lambda$ as depicted in Fig. 2(a) [31]. Here, $\Lambda=H+L$ is the period of the PCs, $\beta=k_0\sin\theta_0$ is the wave vector in the z direction remaining unchanged during propagation in different layers, and θ_0 is the incidence angle. The shaded region in the plot, which is obtained by setting $(M_{11}+M_{22})/2<1$, corresponds to the propagating Bloch modes, while the blank area represents the stopband calculated with $(M_{11}+M_{22})/2>1$ instead. Since all the modes in the free space must obey $\omega=c(k_{x0}^2+\beta^2)^{1/2}$, the entire blank region above the line $\omega=c\beta$ refers to the modes that cannot directly propagate into the PCs from the surrounding air without additional coupling mechanism. Here, c is the speed of light in air and k_{x0} is the x direction wave vector in air. As highlighted in the figure, the wavelength range between the dashed lines going through the open and solid circles ($0.16<\omega\Lambda/2\pi c<0.24$) corresponds to the omnidirectional stopband that will reflect incident light at all angles irrespective of polarizations and is calculated as from 430 nm to 650 nm in terms of wavelength unit. This broad stopband efficiently suppresses the transmission below 650 nm. It can be observed that this omnidirectional stopband is very close to the stopband at normal incidence (the range defined by the dashed lines going through the open circle and square) due to the flat band structure, which leads into the omnidirectional transmission performance with little dispersion at different incident angles. By comparison, the band structure of the PCs consisting of lower refractive index materials (*i.e.* utilizing TiO_2 and SiO_2 as H and L layers, respectively) is also plotted featuring a much steeper slope as presented in Fig. S3 in the ESM, which indicates a significant blue shift of the passband (or stopband) at large angles of incidence and will be discussed in details in the next section. Therefore, it can be concluded that the flat band structure directly results from the high refractive indices of the constituent materials (*i.e.*, a-Si and Si_3N_4), allowing a small refracted angle into the structure according to Snell's law and exhibiting the great angular-insensitive property. In addition, the refractive indices of the materials are also a key factor affecting the stopband bandwidth. As plotted in Fig. 2(b), the dependency of the omnidirectional stopband bandwidth on the low refractive index material (n_L) and refractive index contrast (n_H/n_L) reveals that both large n_L and n_H/n_L are required to achieve a broad omnidirectional stopband.

It is typically challenging to generate wide-angle NIR transmission because the longer cavity thickness to create a resonance at a longer wavelength range is required, resulting in sensitivity to the angle of incidence. To investigate the angular performance of this transmissive-type photonic crystal structure, the calculated and measured angle-resolved transmission spectra are illustrated in Fig. 3(a)-(d) for both TE and TM polarized light. Obviously, the transmission below 650 nm is effectively blocked at all angles, which is in good agreement with the prediction of Fig. 2(a). Due to the high refractive indices of the materials in the design as analyzed in the last section, angular insensitivity up to ±60° are observed regardless of polarizations as indicated by the flat dispersion curves in the plot. The simulation is carried out using transfer matrix method and the measured transmission spectra at different angles are obtained by the spectrophotometer (Cary 7000, Agilent) with angle resolved measurement accessory (UMA). Optical images of the fabricated samples at different observing angles under ambient light illumination are provided in Fig. 3(e), displaying stable mirror reflection appearance over a wide angular range. It further validates the angular insensitive

performance of our designed structures and this outstanding characteristic is highly desired in decoration applications. The corresponding reflection spectra dependence on incidence angles are provided in Fig. S4 in the ESM. For comparison, the simulated angular-dependent transmission spectra of the structure utilizing the lower refractive index materials based on TiO_2 and SiO_2, presenting a blue-shifted transmission profile and hence the degraded colors with increasing incident angles, which are well consistent with the prediction in Fig. S3 in the ESM and Fig. 2(b), are provided in Fig. S5 in the ESM. Hence, compared with the common TiO_2/SiO_2 film stack, the a-Si/Si_3N_4 stack can greatly improve the incident angular performance and dramatically decrease the split for two polarizations. For a wide variety of applications such as spectral analysis and imaging, the filter is desired to have a much sharper NIR transmission to exclude the severe effects caused by the unwanted light at short wavelengths. Thus, the influence of the number of '$H/2LH/2$' unit on the passband (stopband) sharpness is explored. Simulated reflection and transmission spectra for structures consisting of different numbers of stacks are illustrated in Fig. S6 in the ESM. By increasing the stacks, a steeper passband (stopband) that is close to the ideal case for the infinite stacks, which is presented by the band structure in Fig. 2(a), can be achieved. When the stack number reaches 7, the steepness of the spectra almost remains unchanged even if further increasing the number of stacks.

2.3 Decorative NIR-Transmitting Designs

The structure discussed above with great angular-insensitive mirror-like reflection provides one option for decorative uses, *e.g.*, hiding the black holes of NIR sensors that are integral to vehicle cockpits and cell phones. In real applications, other colors in addition to the mirror-like appearance, which are impossible with traditional PCs employing transparent materials, are highly desired. To generate various decorative colors, additional three layers (thin Si_3N_4/a-Si/thick Si_3N_4) are incorporated on top of the proposed ternary PC structures as depicted in Fig. 4(a). Different CMY (cyan, magenta, and yellow) colors can be realized by simply adjusting the thicknesses of the added thin Si_3N_4 and a-Si layers while maintaining the high NIR transmission without changing the bottom PCs as plotted in Fig. 4(b)-(d), respectively. Insets in the figures provide the optical images of three colored devices at normal incidence. The slight discrepancy between the simulated and measured results are due to the thickness variation in the deposition process. The detailed structure configuration of each color is summarized in Table 1. The reflection spectra with sharp dips correspond to distinctive colored appearance of CMY devices with their color coordinates described in the chromaticity diagram as shown in Fig. 4(e). As one potential application of these decorative NIR-transmitting filters is to hide the unappealing appearance of sensors used in vehicles and cell phones and these silicon-based NIR sensors typically work near 900 nm, the optical performance of our proposed devices is evaluated up to 900 nm. On the other hand, our structure can prove high transmission at even longer wavelengths (*e.g.*, 1.2μm, see Fig. S7 in the ESM).

To better understand the mechanism of decorative visibly-opaque but NIR-transmitting structures, the yellow colored design is taken as an example to elucidate the function of each layer. Essentially, the new structure can be effectively simplified into an asymmetric Fabry-Perot cavity by treating the bottom PC stacks as a reflective mirror in the visible, which is illustrated in Fig. 4(a). The yellow color is created by suppressing the reflection in the blue color range (light with wavelength < 500 nm, as shown by the reflection dip @~500 nm in Fig. 4(d)) while maintaining the high reflection intensity of light in the other portion in the visible. The suppression of blue light is due to the perfect absorption of a-Si layers, which can be seen from the near 100% absorption peak of the total absorption spectrum as depicted in Fig. 5(a). This guarantees the low detection noise in NIR sensor applications by blocking the visible transmission but allowing only NIR light to pass the stacks, which is impossible with traditional PC structures based on transparent materials. According to the absorption spectra of each a-Si layer, the absorption is mainly ascribed to the 1st (additionally added 10 nm a-Si) and 2nd a-Si (the top 16 nm a-Si of the bottom PC mirror stacks). By calculating the net phase shifts of the 1st and 2nd a-Si layers, it is interesting to find out that the added thin Si_3N_4 (25 nm) between the bottom PC mirror and the top 10 nm a-Si is an effective phase tuning layer that excites the absorption resonances in the blue color range within the absorptive a-Si layers, thereby generating the reflective yellow color [32, 33]. The absorption resonance occurs when the net phase shift is equal to a multiple of 2π, where the net phase shift involves two reflection phases acquired upon reflection from both the top and bottom interfaces and the propagation phase accumulated within the layer. After adding the thin Si_3N_4 phase tuning layer, two closely positioned absorption resonances are excited within the 1st (#1 @493 nm) and 2nd (@504 nm) a-Si layers as shown in Fig. 5(b), which significantly enhances the short wavelength absorption and are well-consistent with the absorption peaks of the red and blue curves in Fig. 5(a). For comparison, the net phase shift of the top a-Si layer after removing the Si_3N_4 phase tuning layer (in this case the 1st and 2nd a-Si layers will become one single layer) is also plotted in the figure and no absorption resonance exists near 500 nm wavelength. The phase tuning function of the added Si_3N_4 can be further confirmed by the strong reflection dip of the designed yellow colored NIR-transmitting structure when compared to the reflection spectrum of the stacks without the 25 nm Si_3N_4 layer as depicted in Fig. 5(c). On the other hand, the very top thick Si_3N_4 serves as an anti-reflection (AR) layer that maintains the high NIR transmission, which can be clearly observed when comparing the transmission spectra of the stacks with and without the top 140 nm Si_3N_4 in the Fig. 5(c). The AR resonance occurs @728 nm as illustrated by the black solid cure in Fig. 5(b), where the net phase shift of the top Si_3N_4 is equal to a multiple of 2π. Fig. 5(d) provides the calculated electric field distribution inside the yellow device as a function of wavelength. Confined electric field within the short wavelength range inside the 1st and 2nd a-Si layers (#1 and #2 solid circles) corresponds to strong absorption @~500 nm as the optical absorption is directly proportional to the electric field intensity ($\text{Absorption} = (1/2)c\varepsilon_0\alpha n|E(x)|^2$, where c is the speed of light, ε_0 is the permittivity of free space, n is the real part of the refractive index, and is $\alpha = 4\pi\kappa/\lambda$ is the absorption coefficient with κ being the imaginary part of the refractive

index). Absorption resonances also exist inside the other a-Si layers but with much weaker intensities (white dashed circle #A), which are well consistent with the absorption spectra provided in Fig. 5(a). In addition, the strong AR resonance beyond 700 nm inside the top Si_3N_4 effectively induce the NIR transmission as seen from the propagating modes in the underneath layers (black dashed elliptical circle #B). All the information extracted from the electric field distribution plot agrees well with the predictions of Fig. 5(a)-(c), thus validating the phase tuning and AR functions of additionally added thin and thick Si_3N_4 layers, respectively.

Similarly, due to the high refractive indices of both a-Si and Si_3N_4 employed in the designs, all the fabricated CMY colored devices present angular-insensitive performance that is highly-preferred in decorative applications. Fig. 6(a)-(c) provide the calculated angle-resolved reflection spectra of all three colors under unpolarized light illumination, which agree with the measured results presented in Fig. 6(d)-(f). The flat dispersion curves in both simulated and measured plots clearly indicate the excellent omnidirectional properties up to ±60°. Fig. 6(g) presents photographs of fabricated colored samples are taken at several observing directions, further validating the angle-robust decorative appearance.

3 Conclusions

In summary, we have experimentally demonstrated colored visibly-opaque but highly NIR-transmitting filters based on 1D ternary PCs. A wide variety of decorative reflection colors can be created without affecting the high NIR transmission performance, which is impossible with traditional PC structures based on transparent materials. Resulting from the high refractive index contrast between the materials employed in the design as well as the absorption loss of semiconductors, the proposed NIR filter effectively blocks visible transmission with only 7 layers, which is far fewer than conventional schemes. It also exhibits great angle-robust performance up to ±60° irrespective of the polarization state of incident light at both top and back incidence due to the high refractive index of all the involved materials. With the fabrication simplicity where only the deposition step needs to be involved, the presented strategy offers an attractive route towards large-scale structural filters in a variety of applications such as imaging, displays, holography, and especially NIR-sensor decorations.

4 Method

4.1 Device fabrication

Multilayered NIR-transmitting filters based on PCs were fabricated with plasma-enhanced chemical vapor deposition (PECVD) at 260 °C on silica substrates without breaking the chamber.

4.2 Simulation and Measurement

Optical simulations based on transfer matrix method are performed to calculate the transmission/reflection/absorption spectra, phase information, and normalized electric field distributions. The measured angle-resolved transmission spectra and reflection at normal incidence are obtained by the spectrophotometer (Cary 7000, Agilent) with angle resolved measurement accessory (UMA). The measured angle-resolved reflection spectra are attained using a spectroscopic ellipsometer (M-2000, J. A. Woollam). The same ellipsometer is applied to extract the refractive indices of a-Si and Si_3N_4, which are used in the optical simulations.

Acknowledgements

The authors would like to thank the National Science Foundation Grant (CMMI- 1727918) for the partial support of this work. C. Ji acknowledges the support by Rackham Graduate Student Research Grant from the University of Michigan.

Electronic Supplementary Material: Supplementary material (Optical spectra, projected band structures, and angle-resolved transmission of PCs based on TiO_2/SiO_2, refractive indices of materials, angle-resolved reflection spectra of 7-layer PCs based on a-Si/Si_3N_4, optical spectra of a-Si/Si_3N_4 PCs with different numbers of stacks, and transmission spectra of CMY colored NIR-transmitting filters within a broader wavelength range) is available in the online version of this article at http://dx.doi.org/10.1007/s12274-***-****-* (automatically inserted by the publisher).

References

[1] Shcherbakova, D. M.; Verkhusha, V. V. Near-infrared fluorescent proteins for multicolor in vivo imaging. *Nat. Methods* **2013**, *10*, 751-754.

[2] Kim, S.; Lim, Y. T.; Soltesz, E. G.; De Grand, A. M.; Lee, J.; Nakayama, A.; Parker, J. A.; Mihaljevic, T.; Laurence, R. G.; Dor, D. M.; Cohn, L. H.; Bawendi, M. G.; Frangioni, J. V. Near-infrared fluorescent type II quantum dots for sentinel lymph node mapping. *Nat. Biotechnol.* **2003**, *22*, 93-97.

[3] Frangioni, J. V. In vivo near-infrared fluorescence imaging. *Curr. Opin. Chem. Biol.* **2003**, *7*, 626-634.

[4] Park, H.; Crozier, K. B. Multispectral imaging with vertical silicon nanowires. *Sci. Rep.* **2013**, *3*, 2460.

[5] Koyama, S.; Inaba, Y.; Kasano, M.; Murata, T. A Day and Night Vision MOS Imager With Robust Photonic-Crystal-Based RGB-and-IR. *IEEE Trans. Electron Devices* **2008**, *55*, 754-759.

[6] Barone, P. W.; Baik, S.; Heller, D. A.; Strano, M. S. Near-infrared optical sensors based on single-walled carbon nanotubes. *Nat. Mater.* **2004**, *4*, 86-92.

[7] Yuan, L.; Lin, W.; Zhao, S.; Gao, W.; Chen, B.; He, L.; Zhu, S. A Unique Approach to Development of Near-Infrared Fluorescent Sensors for in Vivo Imaging. *J. Am. Chem. Soc.* **2012**, *134*, 13510-13523.

[8] Werle, P.; Slemr, F.; Maurer, K.; Kormann, R.; Mücke, R.; Jänker, B. Near- and mid-infrared laser-optical sensors for gas analysis. *Opt. Lasers Eng.* **2002**, *37*, 101-114.

[9] Ghosh, S.; Cherumukkil, S.; Suresh, C. H.; Ajayaghosh, A. A Supramolecular Nanocomposite as a Near-Infrared-Transmitting Optical Filter for Security and Forensic Applications. *Adv. Mater.* **2017**, *29*, 1703783.

[10] Tucker, R. J. Visibly opaque infrared transmitting optical filter containing a combination of copper and vanadyl phthalocyanine sulfonamides. U.S. Patent 4,039,467A, Aug 2, 1977.

[11] Momose, M.; Todokoro, A. Infrared transmissive thermoplastic composition, and articles formed therefrom. U.S. Patent 7,727,418B2, Jun 1, 2010.

[12] Morgan, M. D.; Horne, W. E.; Sundaram, V.; Wolfe, J. C.; Pendharkar, S. V.; Tiberio, R. Application of optical filters fabricated by masked ion beam lithography. *J. Vac. Sci. Technol. B* **1996**, *14*, 3903-3906.

[13] Heinzel, A.; Boerner, V.; Gombert, A.; Bläsi, B.; Wittwer, V.; Luther, J. Radiation filters and emitters for the NIR based on periodically structured metal surfaces. *J. Mod. Opt.* **2000**, *47*, 2399-2419.

[14] Zhang, J.; Xiao, S.; Jeppesen, C.; Kristensen, A.; Mortensen, N. A. Electromagnetically induced transparency in metamaterials at

near-infrared frequency. *Opt. Express* **2010**, *18*, 17187-17192.

[15] Zhang, S.; Fan, W.; Malloy, K. J.; Brueck, S. R. J.; Panoiu, N. C.; Osgood, R. M. Near-infrared double negative metamaterials. *Opt. Express* **2005**, *13*, 4922-4930.

[16] Sokar, A. A. Z.; Hutter, F. X.; Burghartz, J. N. Generation of red color and near infrared bandpass filters using nano-scale plasmonic structures. In *Proceedings of SPIE Optics + Optoelectronics*, Prague, Czech Republic, 2015, pp 95020U.

[17] Yang, Z.; Zhou, Y.; Chen, Y.; Wang, Y.; Dai, P.; Zhang, Z.; Duan, H. Reflective Color Filters and Monolithic Color Printing Based on Asymmetric Fabry–Perot Cavities Using Nickel as a Broadband Absorber. *Adv. Opt. Mater.* **2016**, *4*, 1196-1202.

[18] Yang, Z.; Chen, Y.; Zhou, Y.; Wang, Y.; Dai, P.; Zhu, X.; Duan, H. Microscopic Interference Full-Color Printing Using Grayscale-Patterned Fabry–Perot Resonance Cavities. *Adv. Opt. Mater.* **2017**, *5*, 1700029.

[19] Macleod, H. A. *Thin-film optical filters*; CRC Press: Boca Raton, FL, USA, 2001.

[20] Hawkins, G. J.; Sherwood, R. E.; Barrett, B. M.; Wallace, M.; Orr, H. J. B.; Matthews, K.; Bisht, S. High-performance infrared narrow-bandpass filters for the Indian National Satellite System meteorological instrument (INSAT-3D). *Appl. Opt.* **2008**, *47*, 2346-2356.

[21] Orr, H. J. B.; Wallace, M.; Dalton, G. B. Near-infrared bandpass filters with improved transparency for 1000nm spectral region using sputtered silicon compound films. In *Proceedings of SPIE Astronomical Telescopes + Instrumentation*, Marseille, France, 2008, pp 701830.

[22] Piegari, A.; Sytchkova, A. K.; Di Sarcina, I.; Bulir, J. Visible and near-infrared filters for miniaturized spectrometers. In *Proceedings of SPIE Astronomical Telescopes + Instrumentation*, Marseille, France, 2008, pp 701855.

[23] Kumar, S. A.; Nagendra, C. L.; Shanbhogue, H. G.; Thutupalli, G. K. M. Near-infrared bandpass filters from Si/SiO2 multilayer coatings. *Opt. Eng.* **1999**, *38*, 368-381.

[24] Lu, J. High Performance Infrared Narrow Band Pass Filters for Infrared Sensors and Systems. In *Proceedings of SENSOR + TEST Conferences 2009*, Nürnberg, Germany, 2009, pp 275-280.

[25] Ohtera, Y.; Onuki, T.; Inoue, Y.; Kawakami, S. Multichannel Photonic Crystal Wavelength Filter Array for Near-Infrared Wavelengths. *J. Lightwave Technol.* **2007**, *25*, 499-503.

[26] Ufford, C.; Baumeister, P. Graphical aids in the use of equivalent index in multilayer-filter design. *J. Opt. Soc. Am.* **1974**, *64*, 329-334.

[27] Petterson, L. A. A.; Roman, L. S.; Inganäs, O. Modeling photocurrent action spectra of photovoltaic devices based on organic thin films. *J. Appl. Phys.* **1999**, *86*, 487-496.

[28] Awasthi, S. K.; Ojha, S. P. Design of a tunable optical filter by using a one-dimensional ternary photonic band gap material. *Prog. Electromagn. Res. M* **2008**, *4*, 117-132.

[29] Winn, J. N.; Fink, Y.; Fan, S.; Joannopoulos, J. D. Omnidirectional reflection from a one-dimensional photonic crystal. *Opt. Lett.* **1998**, *23*, 1573-1575.

[30] Fink, Y.; Winn, J. N.; Fan, S.; Chen, C.; Michel, J.; Joannopoulos, J. D.; Thomas, E. L. A dielectric omnidirectional reflector. *Science* **1998**, *282*, 1679-1682.

[31] Lee, K.-T.; Ji, C.; Banerjee, D.; Guo, L. J. Angular- and polarization-independent structural colors based on 1D photonic crystals. *Laser Photon. Rev.* **2015**, *9*, 354-362.

[32] Song, H.; Guo, L.; Liu, Z.; Liu, K.; Zeng, X.; Ji, D.; Zhang, N.; Hu, H.; Jiang, S.; Gan, Q. Nanocavity Enhancement for Ultra-Thin Film Optical Absorber. *Adv. Mater.* **2014**, *26*, 2737-2743.

[33] Liu, D.; Li, Q. Sub-nanometer planar solar absorber. *Nano Energy* **2017**, *34*, 172-180.

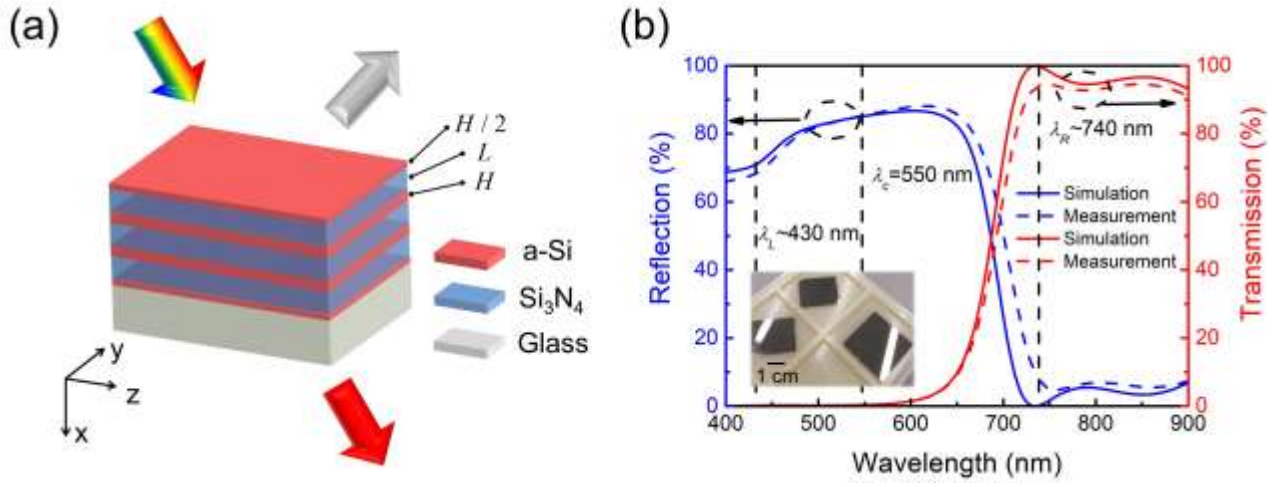

Figure 1 (a) A schematic diagram of the proposed transmissive structure color employing 1D ternary PCs. (b) Simulated and measured spectra of our design. Transmission below 650 nm is greatly suppressed due to both the broad stopband resulting from the high refractive index materials and slight loss of a-Si. The inset at the bottom-left corner is the fabricated samples, showing mirror-like reflection as the visible light is well blocked. The scale bar is 1 cm.

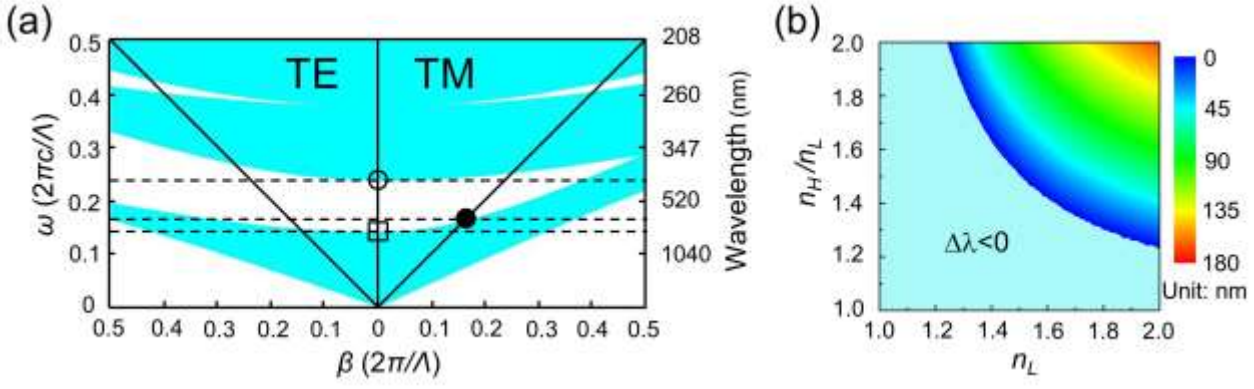

Figure 2 (a) The projected band structures for both TE and TM polarizations calculated from the characteristic matrix of the ternary PCs. (b) Dependency of the omnidirectional stopband of the ternary PCs on the constituent low refractive index material n_L and refractive index contrast n_H / n_L. The region where $\Delta\lambda < 0$ indicates that omnidirectional stopband does not exists in these cases, *i.e.*, no light will be blocked at all angles. The color scale represents the bandwidth of the omnidirectional stopband.

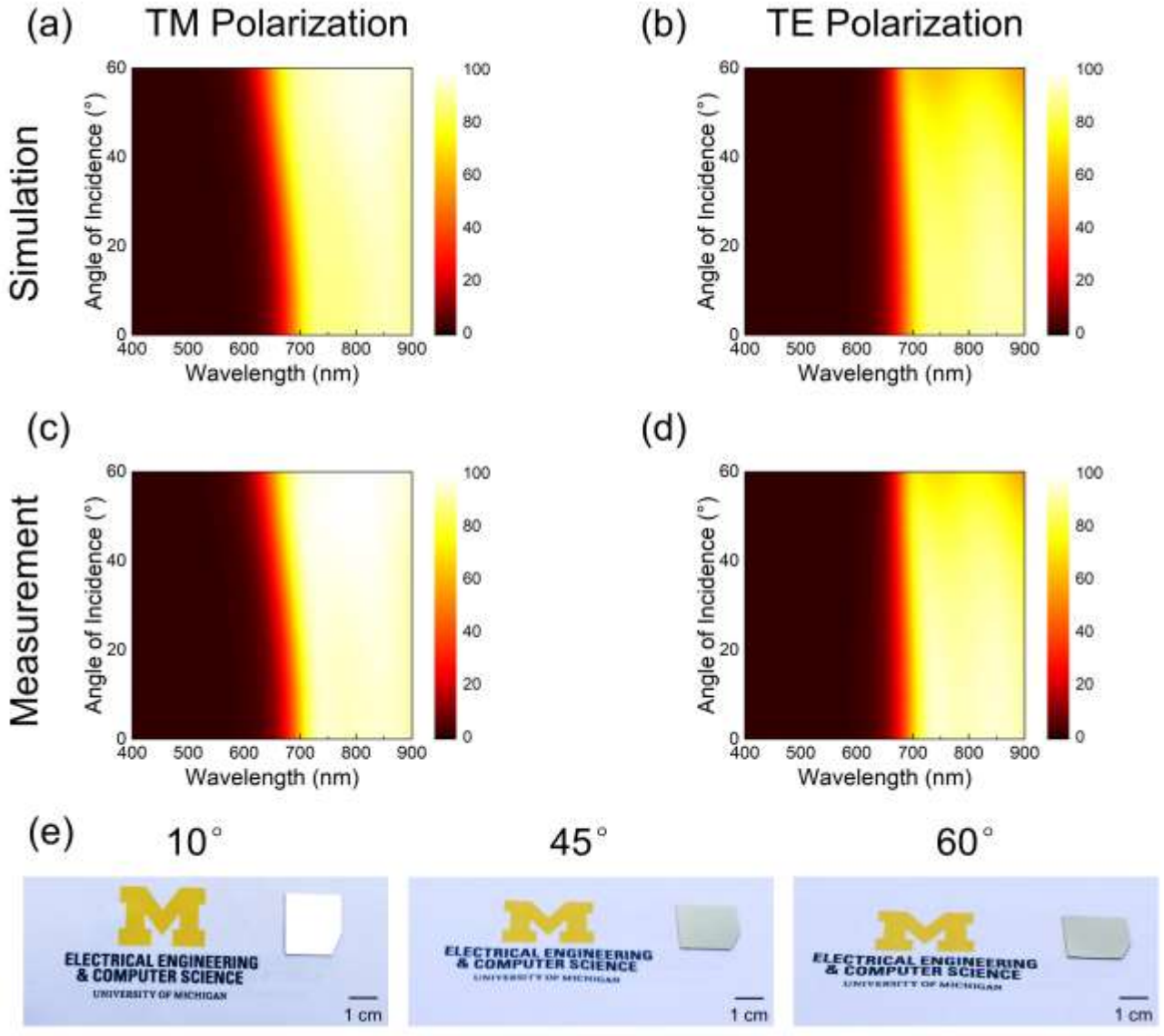

Figure 3 Simulated angle-resolved transmission spectra for (a) TM and (b) TE polarizations, respectively. Measured angle-resolved transmission spectra for (c) TM and (d) TE polarizations, respectively, showing great agreement with the calculated results in (a) and (b). (e) Optical photographs of fabricated samples at different observing angles under ambient light, showing robust mirror-like images over a wide angle range. The scale bars are 1 cm.

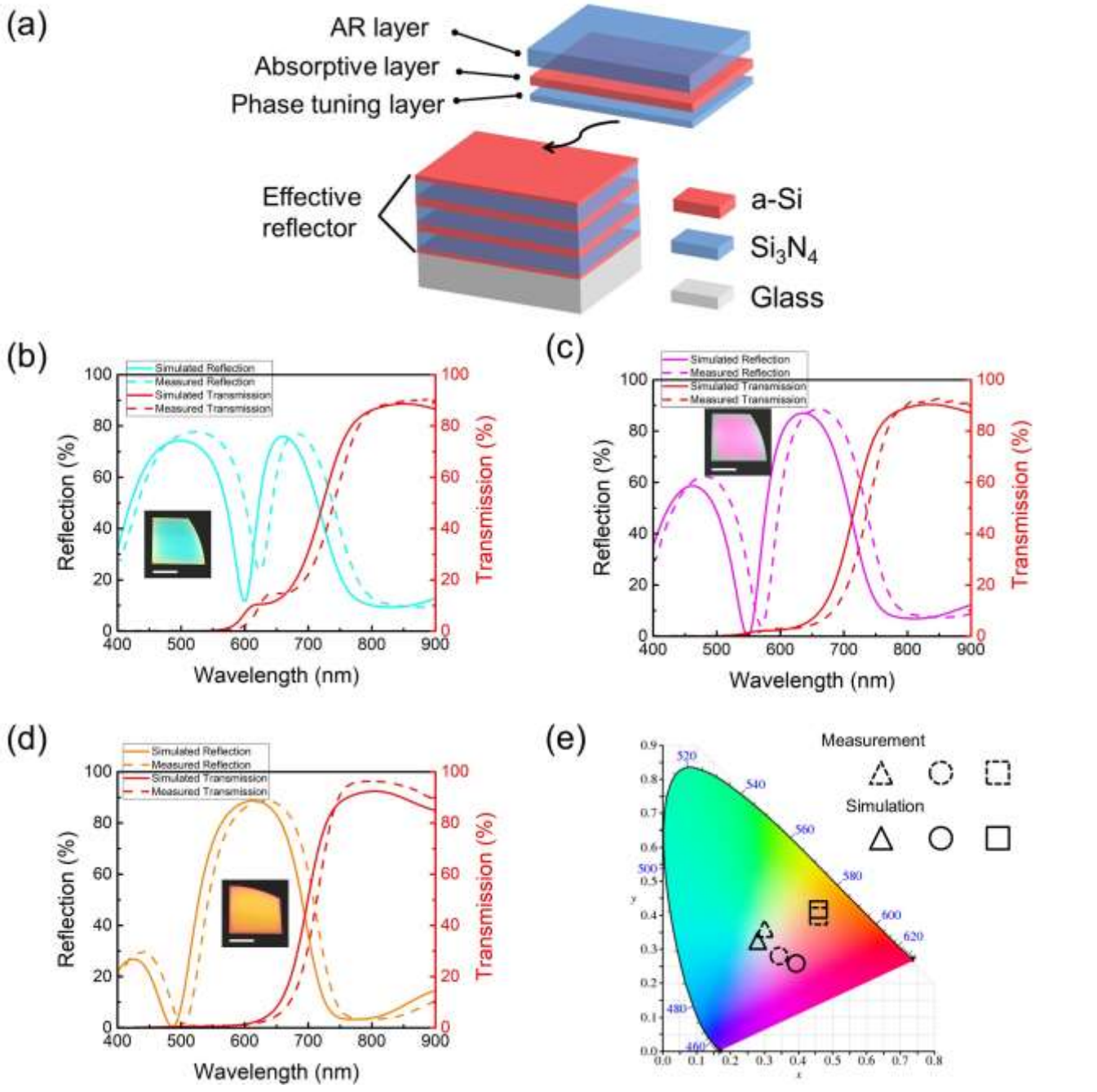

Figure 4 (a) A schematic diagram of new designs for decorative visibly-opaque but NIR-transmitting filters. (b)-(d) Simulated and measured optical performance of CMY colored NIR-transmitting filters. Insets show the optical images of fabricated devices on silica substrates. The scale bars are 1 cm. (e) Colored appearance of decorative NIR-transmitting devices evaluated on the CIE 1931 chromaticity diagram. The color coordinates calculated from the measured reflection spectra of CMY colors are (0.30, 0.36), (0.34, 0.28), and (0.46, 0.38), respectively, showing good match with the simulated results (cyan (0.28, 0.33), magenta (0.39, 0.26), and yellow (0.46, 0.42)).

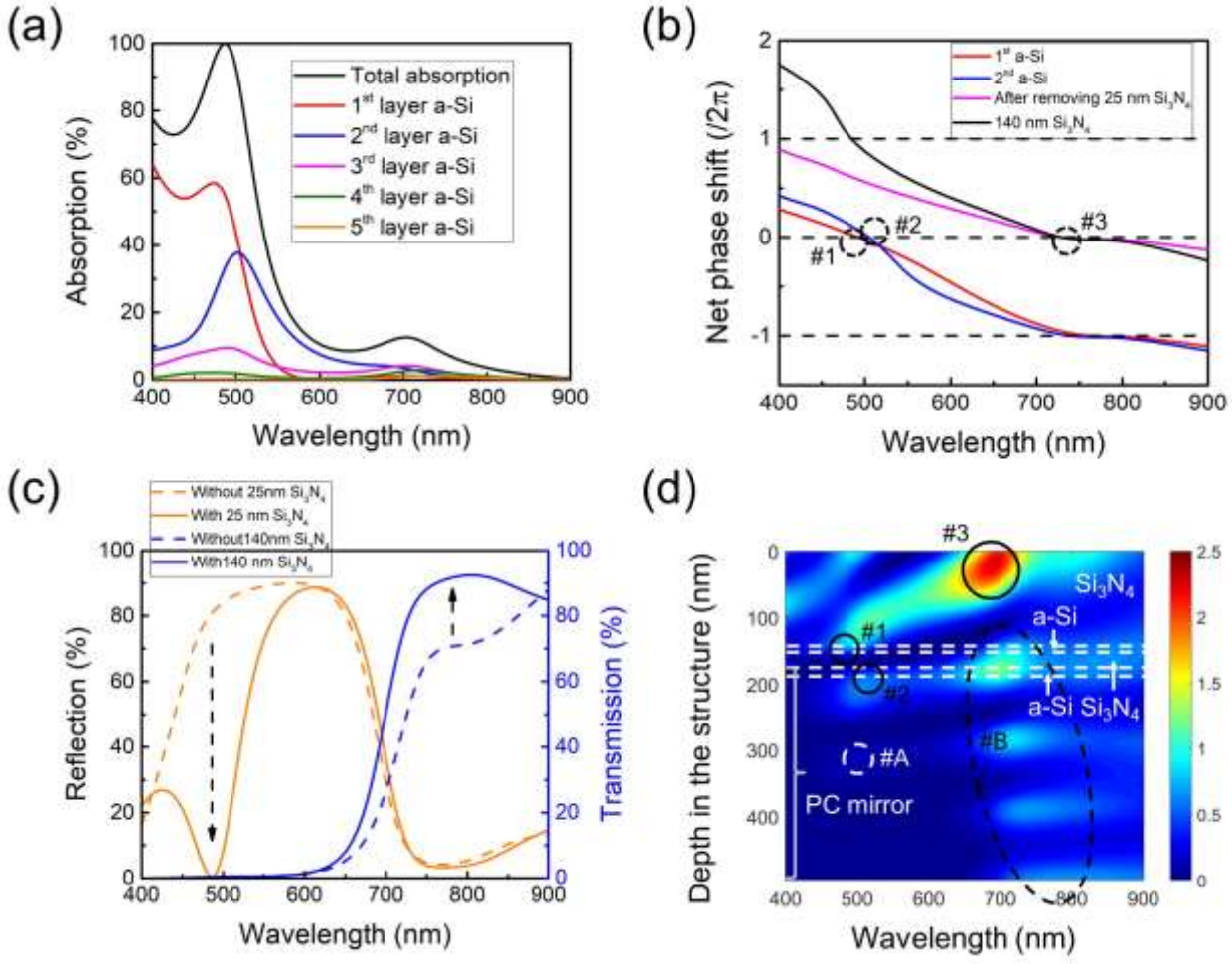

Figure 5 (a) Total absorption spectra and separate absorption in each a-Si layer. The absorption mainly occurs in the 1st and 2nd a-Si layers. (b) Calculated net phase shift, which includes two reflection phase shifts occurring upon both the top and bottom interfaces and the propagation phase accumulation within the layer, analyzing the functions of the additionally added thin and thick Si_3N_4. (c) Spectra comparison of the stacks with and without thin (thick) Si_3N_4, clearly indicating the phase tuning (anti-reflection) function of the added Si_3N_4 layer. (d) Wavelength-dependent electric field distribution inside the whole structure. The strong field in the short wavelength range confined inside the 1st and 2nd a-Si layers directly results in the efficient absorption, thereby generating the decorative color. The additional added 140 nm Si_3N_4 atop effectively induces the strong NIR transmission by exciting AR resonances beyond 700 nm wavelength.

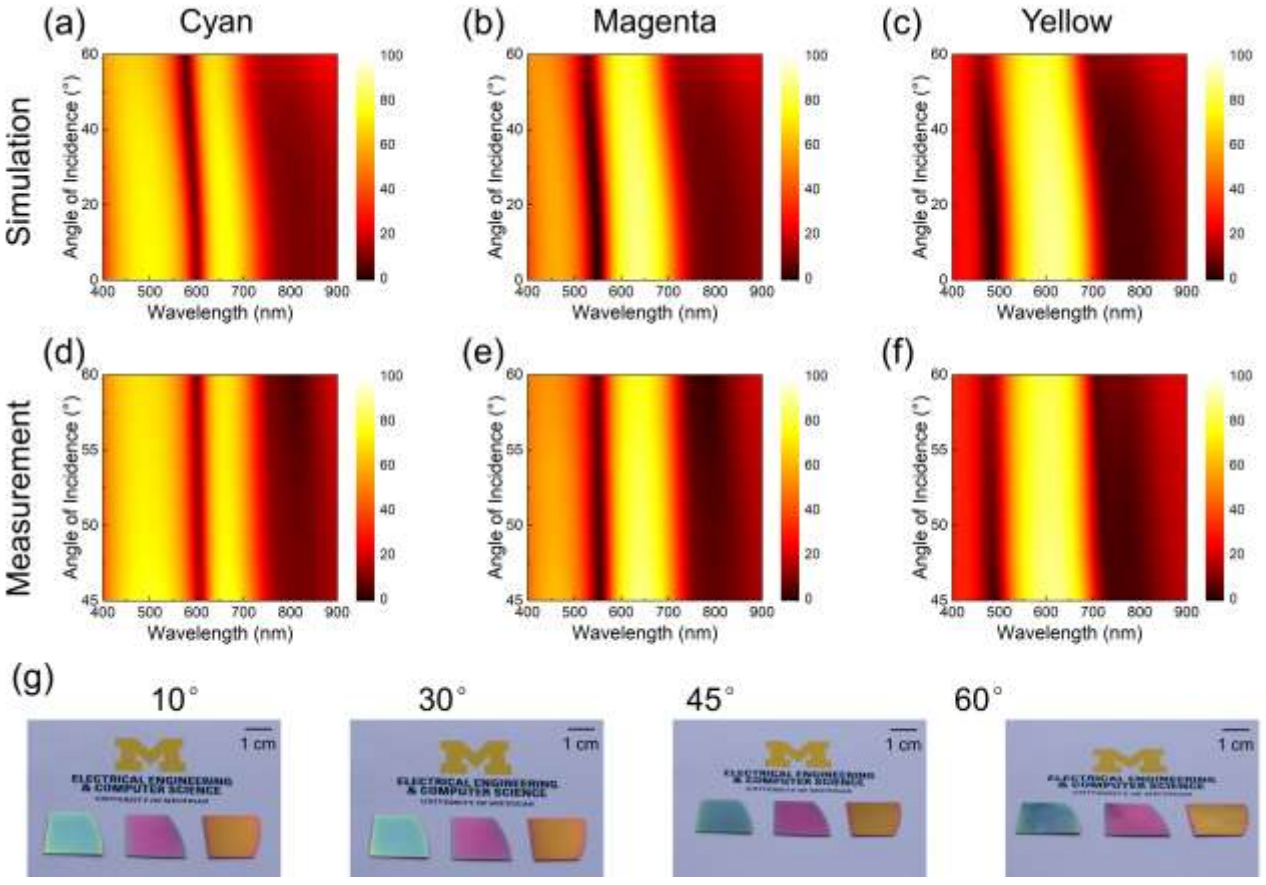

Figure 6 (a)-(c) Simulated angle-resolved reflection spectra for CMY colors under unpolarized light illumination. (d)-(f) The corresponding measured angle-resolved reflection spectra for three colored devices under unpolarized light illumination. The flat dispersion curves in both simulated and measured results indicated the great angular-insensitivity of our proposed structures. (e) Optical images of fabricated CMY colored samples at different observing angles under ambient light, validating the angular-robust colors desired for decorative applications. The scale bars are 1 cm.

Table 1 Structural configurations of CMY colored decorative NIR-transmitting filters. The bottom effective reflectors in all designs employ the same 7-layer PC as presented in Fig. 1(a).

	Thin Si_3N_4 (nm)	a-Si (nm)	Thick Si_3N_4 (nm)
Cyan	45	25	140
Magenta	30	20	140
Yellow	25	10	140

Electronic Supplementary Material

Decorative near-infrared transmission filters featuring high-efficiency and angular-insensitivity employing 1D photonic crystals

Chengang Ji[1,§], Chenying Yang[1,2,§], Weidong Shen[2] (✉), Kyu-Tae Lee[3], Yueguang Zhang[2], Xu Liu[2], and L. Jay. Guo[1] (✉)

[1] *Department of Electrical Engineering and Computer Science, The University of Michigan, Ann Arbor, Michigan 48109, USA*
[2] *State Key Laboratory of Modern Optical Instrumentation, Department of Optical Engineering, Zhejiang University, Hangzhou 310027, China*
[3] *Department of Physics, Inha University, Incheon 22212, Republic of Korea*
[§] *Chengang Ji and Chenying Yang contributed equally to this work*

Supporting information to DOI 10.1007/s12274-****-****-* (automatically inserted by the publisher)

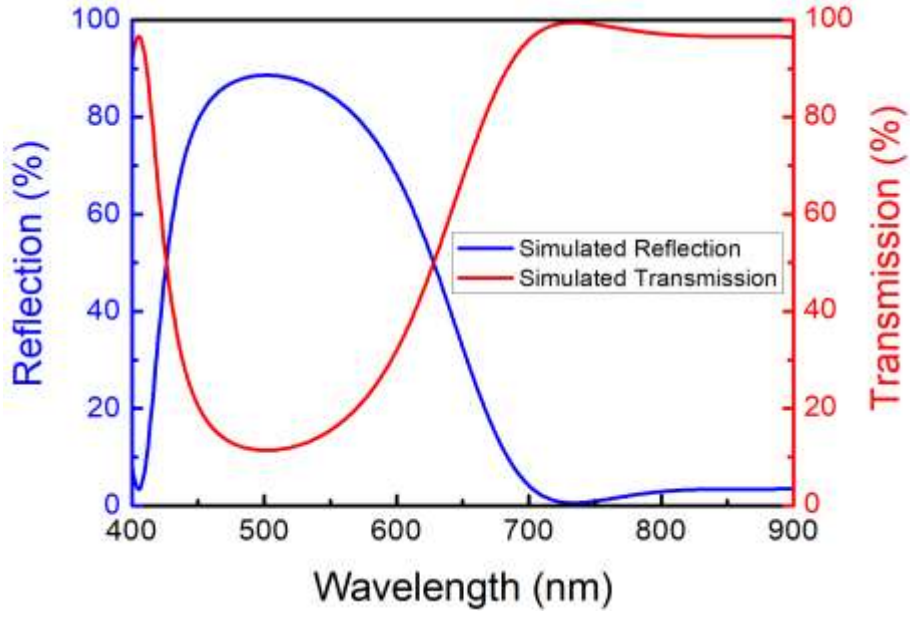

Figure S1 The simulated reflection and transmission spectra of the 7-layered PC structure employing TiO_2 as H layer and SiO_2 as L layer, respectively. It is clear that its stopband bandwidth is much narrower than that of the a-Si/Si_3N_4 stacks, and there is more visible light transmission.

Address correspondence to L. Jay Guo, guo@umich.edu; Weidong Shen, adongszju@hotmail.com

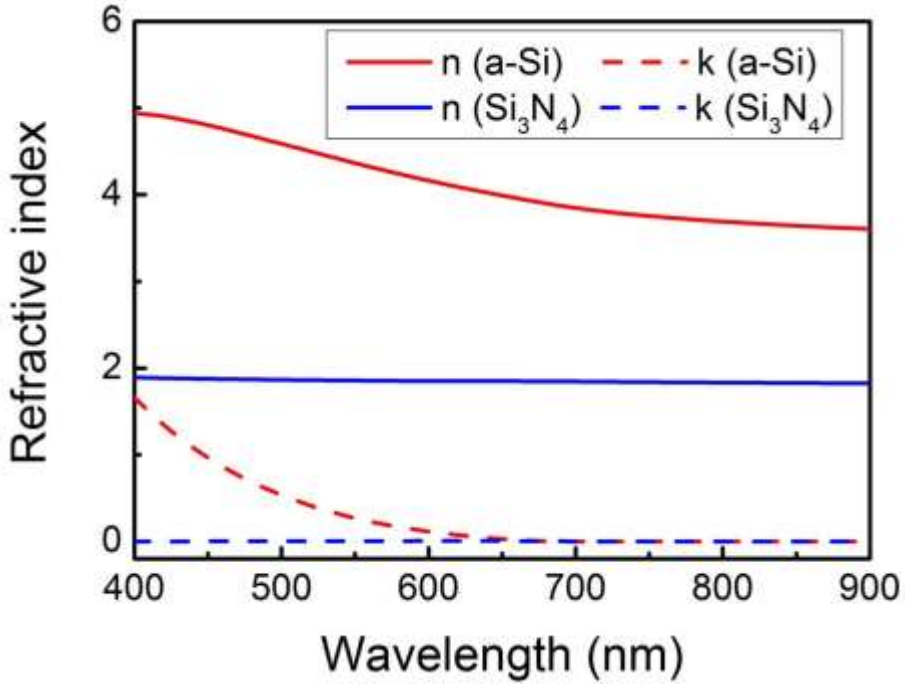

Figure S2 Refractive indices of the constituent materials a-Si and Si_3N_4, measured by a spectroscopic ellipsometer (M-2000, J. A. Woollam).

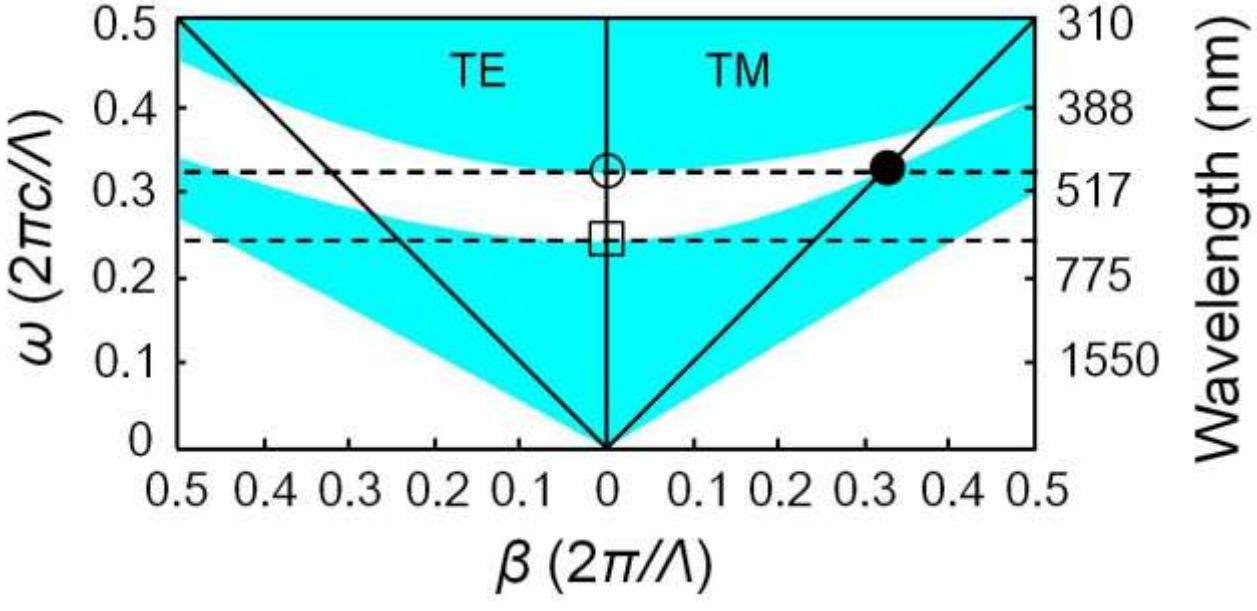

Figure S3 The projected band structure for the ternary PCs made up of TiO_2 as H layer and SiO_2 as L layer. The omnidirectional stopband shrinks close to zero for this combination of low refractive index materials (the wavelength range between the dashed lines going through the open and solid circles) and it is totally different from the stopband bandwidth at normal incidence (the range between the dashed lines going through the open circle and square). This indicates the highly angular sensitive performance of the transmission spectra as shown in Fig. S5.

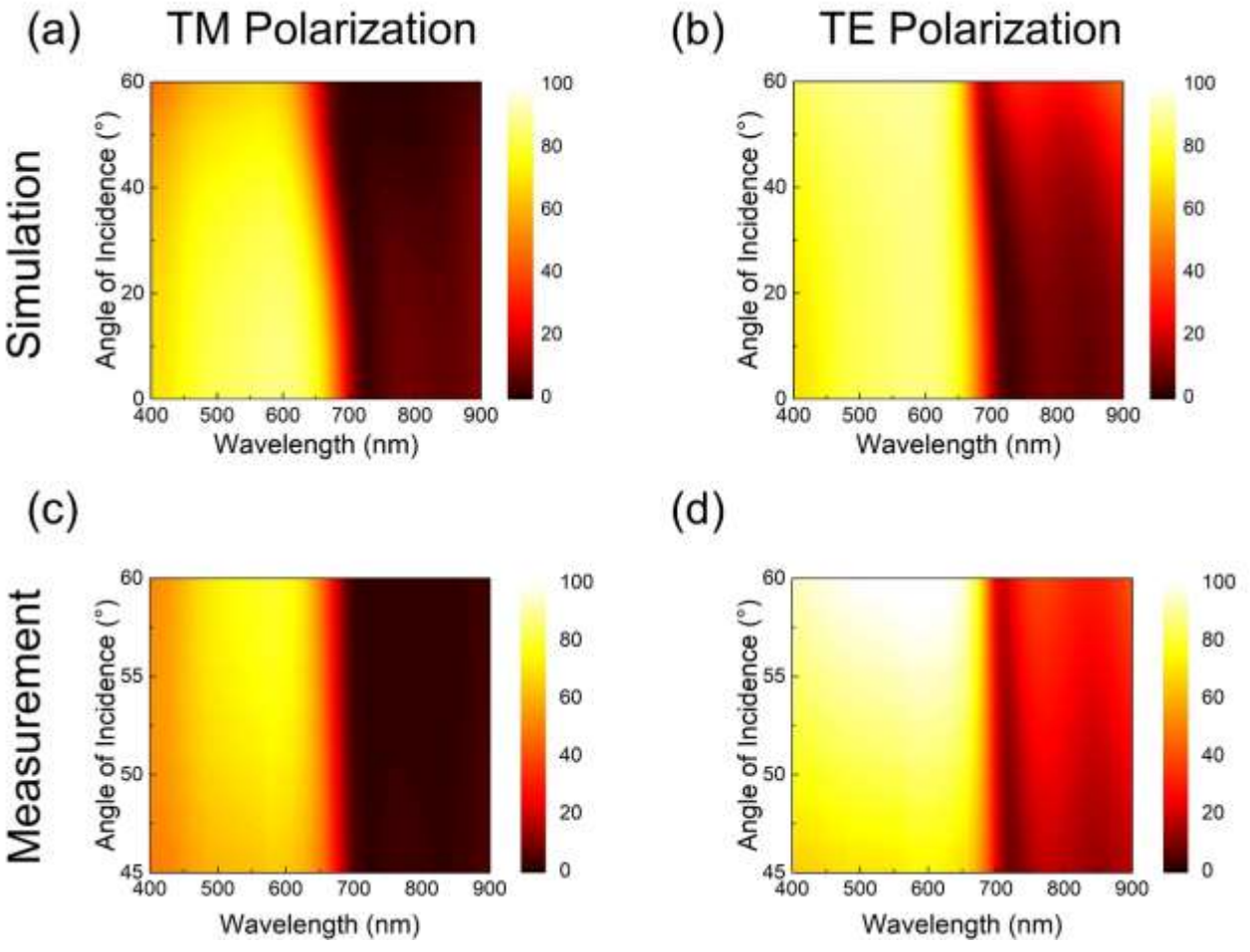

Figure S4 Simulated angle-resolved reflection spectra for (a) TM and (b) TE polarizations, respectively. Measured angle-resolved reflection spectra for (c) TM and (d) TE polarizations, respectively. The flat dispersion curves indicate the great angular-insensitive performance of fabricated samples.

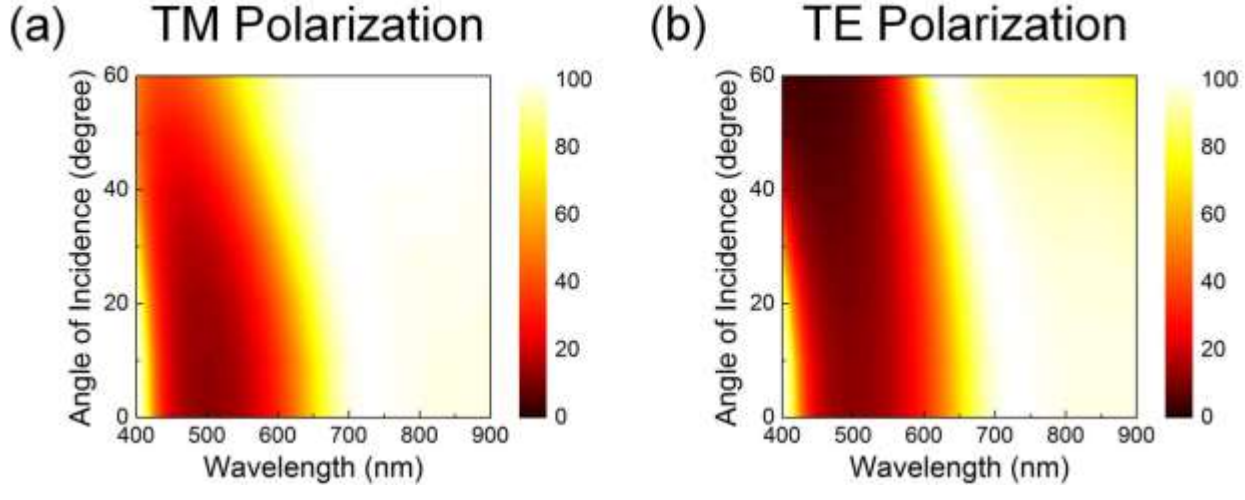

Figure S5 Simulated angular resolved transmission spectra for ternary PCs consisting of low index materials (*i.e.* utilizing TiO_2 and silicon dioxide SiO_2 as H and L layers, respectively) for (a) TM and (b) TE polarizations, respectively. Obvious blue shift of the transmission band can be observed at large incident angles. Here H = 60 nm and L = 95 nm by remaining the central wavelength of the stopband unchanged as λ_c = 550 nm.

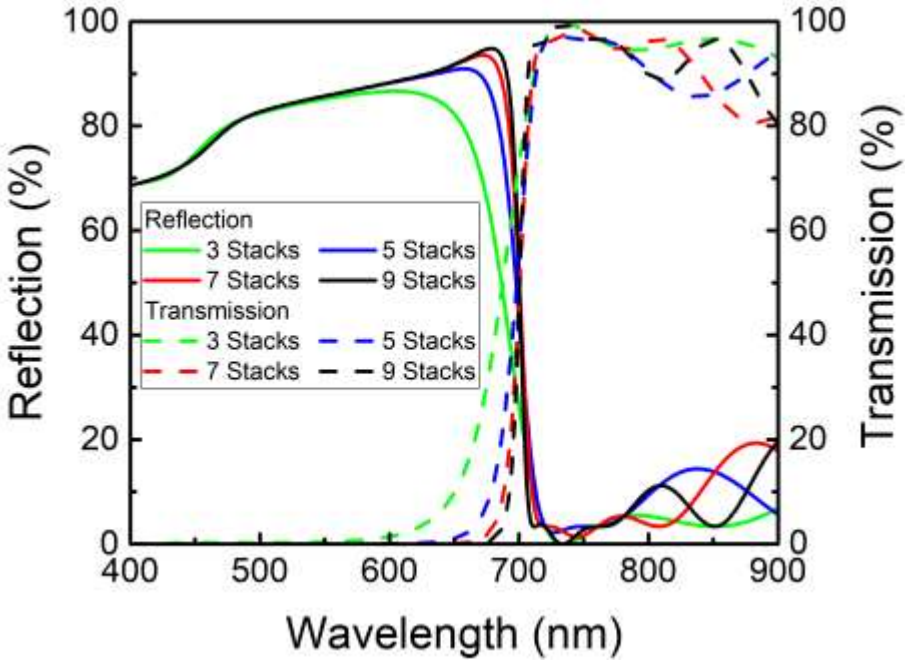

Figure S6 Investigation of the reflection and transmission spectra performance with different numbers of '$H/2LH/2$' stacks. The steepness of the spectra remains unchanged when the stack number reaches 7.

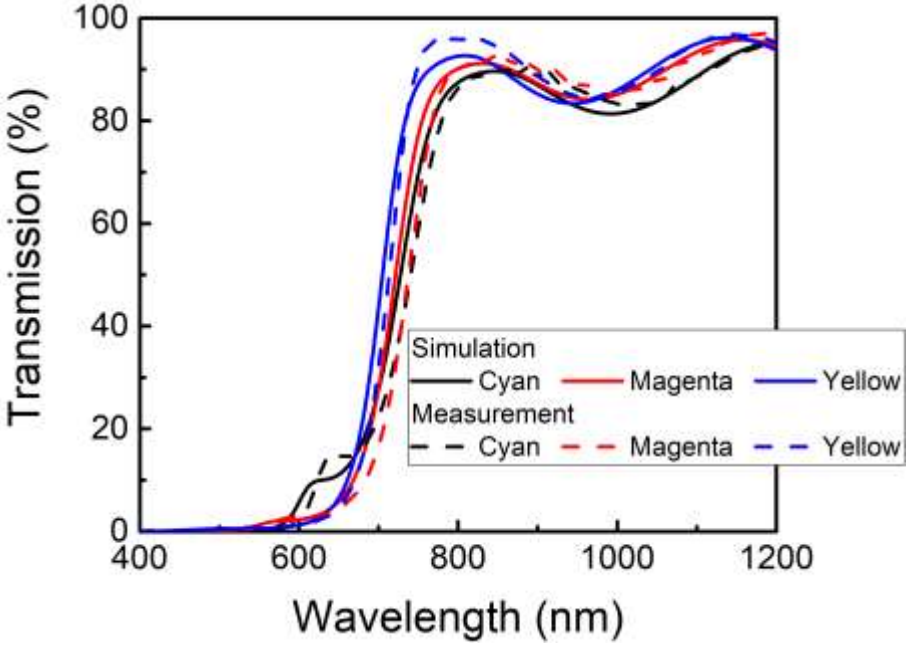

Figure S7 Transmission spectra of our proposed CMY colored devices within a broader wavelength range. High NIR transmission can be maintained to 1200 nm for all the structures, which indicates the possibility of our devices in more applications.